Journal of Computational Physics **182,** 392–417 (2002)
doi:10.1006/jcph.2002.7174

Image-Charge Method for Contour Dynamics in Systems with Cylindrical Boundaries

Gianni G. M. Coppa, Fabio Peano, and Federico Peinetti

Istituto Nazionale per la Fisica della Materia (INFM) and Dipartimento di Energetica, Politecnico di Torino, Corso Duca degli Abruzzi 24, 10129 Torino, Italy
E-mail: ggmcoppa@polito.it, peano@polito.it, peinetti@polito.it

Received April 24, 2002; revised August 5, 2002

In the paper, the classic contour dynamics method for the study of inviscid two-dimensional flow in an infinite domain is extended to systems with a circular boundary. A suitable use of the image-charge technique allows one to express the velocity on the contour of each vortex in terms of line integrals on the contours. Results are presented in the framework of the dynamics of non-neutral plasmas in a Penning trap (the problem is isomorphic to the classic fluid-dynamics problem for a Euler fluid), showing the high accuracy attainable with the method. © 2002 Elsevier Science (USA)

Key Words: contour dynamics; cylindrical boundary; image-charge technique; non-neutral plasmas.

1. INTRODUCTION

Contour dynamics (CD) is a technique originally introduced by Deem and Zabusky [1] and by Zabusky *et al.* [2] to study two-dimensional unbounded flows for inviscid, incompressible fluids, in an infinite domain. The starting point for the CD method is the two-dimensional Euler equations

$$\begin{cases} \dfrac{\partial \Omega_z(r,\theta,t)}{\partial t} + \mathbf{v}(r,\theta,t) \cdot \dfrac{\partial \Omega_z(r,\theta,t)}{\partial \mathbf{r}} = 0 \\ \mathbf{v}(r,\theta,t) = \hat{\mathbf{e}}_z \times \dfrac{\partial \psi(r,\theta,t)}{\partial \mathbf{r}} \\ \nabla^2 \psi(r,\theta,t) = \Omega_z(r,\theta,t) \end{cases} \tag{1}$$

written in terms of the z-component of the vorticity field, $\Omega_z(\Omega = \nabla \times \mathbf{v}$, being $\mathbf{v}$ the velocity field), and the stream function, ψ. According to the method, the domain is divided into regions (vortices) in which the vorticity field is constant. The CD algorithm evaluates directly the velocity field along each vortex contour, without calculating the stream function; in this way, the time evolution of the contours can be calculated.

0021-9991/02 $35.00

An improved CD algorithm, called "countour Surgery," was developed by Dritschel [3], who proposed a more refined method for the contour discretization. By taking into account small-scale effects, a better description of the contours is obtained, thus making possible the study of complex contour configurations. Van Buskirk *et al.* [4] also developed a different CD algorithm for unbounded flows, which makes use of a spectral representation of each vortex contour.

In all the works just cited, the velocity field is expressed as a sum of suitable line integrals along the contour of each vortex. The CD method does not use any spatial computational grid, thus avoiding the typical inaccuracies of the space discretization and allowing high spatial resolution in the solution. This important result can be achieved because the Green's function of the Poisson equation for an unbounded system, $G(\mathbf{r}' \to \mathbf{r})$, satisfies the property

$$\frac{\partial G}{\partial \mathbf{r}'} = -\frac{\partial G}{\partial \mathbf{r}}, \tag{2}$$

which is no longer valid for bounded systems.

The present work deals with the generalization of the CD method to physical systems having a circular boundary. The motivation for this study was initially given by its applications to non-neutral plasmas confined by a Penning trap. In fact, the charge density $\rho(r, \theta, t)$ confined in the central region of a Penning trap evolves in time according to the mathematical model [5]

$$\begin{cases} \dfrac{\partial \rho}{\partial t} + \mathbf{v}(r, \theta, t) \cdot \dfrac{\partial \rho(r, \theta, t)}{\partial \mathbf{r}} = 0 \\ \mathbf{v}(r, \theta, t) = \dfrac{1}{B_0} \hat{\mathbf{e}}_z \times \dfrac{\partial \phi(r, \theta, t)}{\partial \mathbf{r}} \\ \nabla^2 \phi(r, \theta, t) = -\dfrac{1}{\varepsilon_0} \rho(r, \theta, t) \\ \phi(r = R) = 0 \\ \rho(r, \theta, 0) = \rho_0(r, \theta), \end{cases} \tag{3}$$

where ρ is the charge density field, ϕ is the electrostatic potential, R is the radius of the trap, B_0 is the external magnetic field, and ε_0 is the vacuum dielectric constant.

The model (3), comprising the continuity equation, in which the velocity field is given by the $\mathbf{E} \times \mathbf{B}$ drift, and the Poisson equation, is clearly isomorphic to the model (1) used in fluid dynamics. Although the present work focuses on non-neutral plasmas applications, such isomorphism provides an immediate extension of the results to fluid-dynamics studies with the same geometry.

A widely used technique for solving Eqs. (3) is the particle-in-cell (PIC) method, which uses a set of finite-size computational particles to describe the plasma distribution and a spatial computational grid for the numerical solution of the Poisson equation. The CD methods take into account only piecewise-constant density profiles and, if a very high precision in the solution is required, they are in general rather time consuming compared to the PIC method; however, the absence of a spatial discretization allows a very high resolution in the simulation. Thus, contour dynamics cannot be regarded as an alternative to the PIC method, but it can lead to extremely precise solutions, which can be considered as reference results. For instance, contour dynamics can be successfully used in accurate nonlinear studies of instabilities for hollow density profiles [6].

To solve Eqs. (3) within the framework of CD, a new algorithm has to be developed, as the Green's function for the Poisson equation does not satisfy property (2). A way of extending the CD technique to study non-neutral plasmas in a Penning trap has been proposed by Backhaus *et al.* [7, 8], who employed an expression for the electrostatic potential ϕ of

$$\phi = \phi_p + \phi_0, \tag{4}$$

where ϕ_p is evaluated using the Green's function for unbounded systems, while ϕ_0 is the solution of the Laplace equation, $\nabla^2\phi_0 = 0$, with boundary conditions

$$\phi_0(R, \theta) = -\phi_p(R, \theta). \tag{5}$$

The potential ϕ_0 is expressed in terms of a Fourier expansion with respect to θ, as

$$\phi_0(r, \theta) = \sum_{l=-\infty}^{+\infty} \left(\frac{r}{R}\right)^{|l|} D_l e^{-il\theta}, \tag{6}$$

where the coefficients D_l, to be determined so as to satisfy condition (5), are written in terms of suitable contour integrals; for the calculations, the sum is truncated at some maximum value of l. Once the electrostatic potential ϕ is obtained, the velocity field is readily calculated.

In the following, an alternative method based on the image-charge technique is proposed. In this way, a fully analytic expression for the velocity field is obtained, without the need to calculate the electrostatic potential. The method is presented in detail for plasmas or ideal fluids evolving in the interior domain defined by a cylindrical boundary. However, with minor adjustments, the technique also can be used for studying the dynamics of external flows.

2. ANALYTIC DETERMINATION OF THE VELOCITY FIELD

In the point-vortex theory [5], the cylindrical boundary conditions can be taken into account by associating each vortex of charge $+q$ and coordinates (r, θ) with an image vortex of charge $-q$ and coordinates $(R^2/r, \theta)$: By doing so, the calculations can be carried out as for an infinite domain. This approach is still employable when dealing with vortices of finite extension: If the charge density $\rho(r, \theta)$ is assigned within the cylindrical domain, each elementary charge $\rho(r, \theta)\, r\, dr\, d\theta$ induces a corresponding image elementary charge of

$$\hat{\rho}(r', \theta')\, r' dr' d\theta' = -\rho(r, \theta)\, r\, dr\, d\theta, \tag{7}$$

where

$$r' = \frac{R^2}{r}, \quad \theta' = \theta. \tag{8}$$

Referring to vortices of constant charge density, in which

$$\rho(\mathbf{r}) = \begin{cases} \rho_0, & \mathbf{r} \in D \\ 0, & \mathbf{r} \notin D \end{cases} \tag{9}$$

(D is the region of the domain occupied by the plasma) and using Eq. (8), one obtains

$$\hat{\rho}(\mathbf{r}') = \begin{cases} -\rho_0 \left(\frac{R}{r'}\right)^4, & \mathbf{r}' \in \hat{D} \\ 0, & \mathbf{r}' \notin \hat{D}, \end{cases} \tag{10}$$

where $\hat{D}$ is the image region associated with D.

The electrostatic potential can be written as the sum of two terms,

$$\phi(\mathbf{r}) = \int_D G(\mathbf{r}' \to \mathbf{r}) \rho_0 \, d\mathbf{r}' + \int_{\hat{D}} G(\mathbf{r}' \to \mathbf{r}) \hat{\rho}(\mathbf{r}') \, d\mathbf{r}' = \phi_1(\mathbf{r}) + \phi_2(\mathbf{r}), \tag{11}$$

the first is related to the real charge distribution (region D) and the second to the image (region $\hat{D}$), with $G(\mathbf{r}' \to \mathbf{r})$ being the Green's function of the $2D$ Poisson equation in an infinite domain:

$$G(\mathbf{r}' \to \mathbf{r}) = -\frac{1}{2\pi\varepsilon_0} \log(|\mathbf{r}' - \mathbf{r}|). \tag{12}$$

To evaluate the gradient of Eq. (11), one can observe that the first term,

$$\frac{\partial \phi_1}{\partial \mathbf{r}} = \rho_0 \int_D \frac{\partial}{\partial \mathbf{r}} G(\mathbf{r}' \to \mathbf{r}) \, d\mathbf{r}' = -\rho_0 \int_D \frac{\partial}{\partial \mathbf{r}'} G(\mathbf{r}' \to \mathbf{r}) \, d\mathbf{r}', \tag{13}$$

can be rewritten as a contour integral using the divergence theorem, according to the classic CD approach, as

$$\frac{\partial \phi_1}{\partial \mathbf{r}} = \left(-\rho_0 \oint_{\partial D} G(\mathbf{r}' \to \mathbf{r}) n'_x \, dl' \right) \hat{\mathbf{e}}_\mathbf{x} + \left(-\rho_0 \oint_{\partial D} G(\mathbf{r}' \to \mathbf{r}) n'_y \, dl' \right) \hat{\mathbf{e}}_\mathbf{y}. \tag{14}$$

The gradient of the second term of Eq. (11) cannot be manipulated in the same way: In fact, the image density field $\hat{\rho}(\mathbf{r}')$ is not constant in the region $\hat{D}$ and therefore $G(\mathbf{r}' \to \mathbf{r})\hat{\rho}(\mathbf{r}')$ does not satisfy property (2). However, this term can be reduced analytically to a contour integral, thus extending the standard CD approach to cylindrically bounded systems. In fact, the expression for $\partial\phi_2/\partial\mathbf{r}$ can be rearranged as follows:

$$\frac{\partial \phi_2}{\partial \mathbf{r}} = -\int_{\hat{D}} \frac{\partial}{\partial \mathbf{r}'} [G(\mathbf{r}' \to \mathbf{r}) \hat{\rho}(\mathbf{r}')] \, d\mathbf{r}' + \int_{\hat{D}} G(\mathbf{r}' \to \mathbf{r}) \frac{\partial}{\partial \mathbf{r}'} [\hat{\rho}(\mathbf{r}')] \, d\mathbf{r}' = \frac{\partial \phi_2^I}{\partial \mathbf{r}} + \frac{\partial \phi_2^{II}}{\partial \mathbf{r}}. \tag{15}$$

The term $\partial\phi_2^I/\partial\mathbf{r}$ can be readily rearranged to obtain the more convenient expression

$$\frac{\partial \phi_2^I}{\partial \mathbf{r}} = -\left(\oint_{\partial \hat{D}} G(\mathbf{r}' \to \mathbf{r}) \hat{\rho}(\mathbf{r}') n'_x \, dl' \right) \hat{\mathbf{e}}_x - \left(\oint_{\partial \hat{D}} G(\mathbf{r}' \to \mathbf{r}) \hat{\rho}(\mathbf{r}') n'_y \, dl' \right) \hat{\mathbf{e}}_y \tag{16}$$

while the second term needs a different approach: Observing that

$$\frac{\partial [\hat{\rho}(\mathbf{r}')]}{\partial \mathbf{r}'} = \begin{cases} 4\rho_0 \dfrac{R^4}{r'^5} \hat{\mathbf{e}}_{r'}, & \mathbf{r}' \in \hat{D} \\ 0, & \mathbf{r}' \notin \hat{D} \end{cases} \tag{17}$$

one can rewrite the components of $\partial\phi_2^{II}/\partial\mathbf{r}$ can as

$$\frac{\partial\phi_2^{II}}{\partial\mathbf{r}}\cdot\hat{\mathbf{e}}_r = \int_{\hat{D}} G(\mathbf{r}'\to\mathbf{r})\frac{d\hat{\rho}}{dr'}\hat{\mathbf{e}}_r\cdot\hat{\mathbf{e}}_{r'}\,d\mathbf{r}' \tag{18a}$$

$$\frac{\partial\phi_2^{II}}{\partial\mathbf{r}}\cdot\hat{\mathbf{e}}_\theta = \int_{\hat{D}} G(\mathbf{r}'\to\mathbf{r})\frac{d\hat{\rho}}{dr'}\hat{\mathbf{e}}_\theta\cdot\hat{\mathbf{e}}_{r'}\,d\mathbf{r}', \tag{18b}$$

where

$$\hat{\mathbf{e}}_r\cdot\hat{\mathbf{e}}_{r'} = \cos(\theta'-\theta),\quad \hat{\mathbf{e}}_\theta\cdot\hat{\mathbf{e}}_{r'} = \sin(\theta'-\theta),\quad \frac{d\hat{\rho}}{dr'} = 4\rho_0\frac{R^4}{r'^5}. \tag{19}$$

The integrals appearing in Eqs. (18a) and (18b) can be written as contour integrals by introducing a new function, $\psi(\mathbf{r},\mathbf{r}')$, which satisfies the condition

$$G(\mathbf{r}'\to\mathbf{r})\frac{d\hat{\rho}}{dr'} = \frac{1}{r'}\frac{\partial}{\partial r'}(r'\psi(\mathbf{r},\mathbf{r}')), \tag{20}$$

in order to write

$$\frac{\partial\phi_2^{II}}{\partial\mathbf{r}}\cdot\hat{\mathbf{e}}_r = \oint_{\partial\hat{D}}\psi(\mathbf{r},\mathbf{r}')\cos(\theta'-\theta)n_r'\,dl' \tag{21a}$$

$$\frac{\partial\phi_2^{II}}{\partial\mathbf{r}}\cdot\hat{\mathbf{e}}_\theta = \oint_{\partial\hat{D}}\psi(\mathbf{r},\mathbf{r}')\sin(\theta'-\theta)n_r'\,dl'. \tag{21b}$$

By solving Eq. (20), the analytic expression of $\psi(\mathbf{r},\mathbf{r}')$ is obtained as

$$\begin{aligned} r'\psi(\mathbf{r},\mathbf{r}') &= -\int_{r'}^{+\infty} r'G(\mathbf{r}'\to\mathbf{r})\frac{d\hat{\rho}}{dr'}\,dr' \\ &= -\alpha\int_{r'}^{+\infty}\frac{\log[r'^2+r^2-2rr'\cos(\theta'-\theta)]}{r'^4}\,dr', \end{aligned} \tag{22}$$

where $\alpha = -\rho_0R^4/\pi\varepsilon_0$. After calculating the integral (22), $r'\psi(\mathbf{r},\mathbf{r}')$ can be expressed as

$$r'\psi(\mathbf{r},\mathbf{r}') = H(\mathbf{r},\mathbf{r}') + \frac{\alpha}{3}[K(r') + Q(\mathbf{r},\mathbf{r}')W(r,\theta,\theta')] - \frac{\pi\alpha W(r,\theta,\theta')}{6r|\sin(\theta'-\theta)|}, \tag{23}$$

where

$$H(\mathbf{r},\mathbf{r}') = \left(-\frac{\alpha}{3r'^3} - \frac{\alpha C}{6}\right)\log[r'^2+r^2-2rr'\cos(\theta'-\theta)] \tag{24}$$

$$Q(\mathbf{r},\mathbf{r}') = \frac{1}{r\sin(\theta'-\theta)}\arctan\left[\frac{r'-r\cos(\theta'-\theta)}{r\sin(\theta'-\theta)}\right] \tag{25}$$

$$W(r,\theta,\theta') = (D - Cr\cos(\theta'-\theta)),\quad K(r') = C\log r' - \frac{B}{r'} - \frac{A}{2r'^2} \tag{26}$$

$$\begin{aligned} A &= -\frac{2}{r}\cos(\theta'-\theta),\quad B = \frac{2+2Ar\cos(\theta'-\theta)}{r^2} \\ C &= \frac{2Br\cos(\theta'-\theta)-A}{r^2},\quad D = 2Cr\cos(\theta'-\theta) - B. \end{aligned} \tag{27}$$

As Eq. (22) shows, $r'\psi(\mathbf{r}, \mathbf{r}')$ tends to zero for $r' \to +\infty$ and, consequently, the image contribution to the velocity field vanishes when the image distribution approaches infinity.

Once $\psi(\mathbf{r}, \mathbf{r}')$ is determined, $\partial\phi/\partial\mathbf{r}$ can be expressed as a sum of contour integrals as

$$\frac{\partial\phi}{\partial\mathbf{r}} = \frac{\partial\phi_1}{\partial\mathbf{r}} + \frac{\partial\phi_2^I}{\partial\mathbf{r}} + \frac{\partial\phi_2^{II}}{\partial\mathbf{r}}, \tag{28}$$

and the velocity field is readily evaluated from the second of Eqs. (3).

If the contours are described by means of a finite set of points $\{\mathbf{r}_p\}$, $p = 1, \ldots N$, the analytic expression for the velocity field deduced here can be formally written as

$$\mathbf{v}(\mathbf{r}) = \mathbf{f}(\mathbf{r}, \{\mathbf{r}_p\}). \tag{29}$$

Thus, the evolution of the contours is governed by the following system of differential equations:

$$\begin{cases} \dfrac{d\mathbf{r}_1}{dt} = \mathbf{f}(\mathbf{r}_1, \{\mathbf{r}_p\}) \\ \dfrac{d\mathbf{r}_2}{dt} = \mathbf{f}(\mathbf{r}_2, \{\mathbf{r}_p\}) \\ \vdots \\ \dfrac{d\mathbf{r}_N}{dt} = \mathbf{f}(\mathbf{r}_N, \{\mathbf{r}_p\}). \end{cases} \tag{30}$$

An alternative (and more general) technique consists of describing the contours by means of analytic curves, whose shape depends on a set of N_c coefficients $\{C_\alpha\}$. (For example, in some situations a vortex can be approximated as an ellipse; in this case, five coefficients are needed.) Now the velocity field can be formally written as

$$\mathbf{v}(\mathbf{r}) = \mathbf{g}(\mathbf{r}, \{C_\alpha\}). \tag{31}$$

Moreover, a mathematical procedure (e.g., a least-square technique) must be defined to calculate the coefficients $\{C_\alpha\}$ of the analytic curves that best fit a generic set of $\{\mathbf{r}_p\}$ contour points. In general, this procedure can be written as

$$C_\alpha = h_\alpha(\{\mathbf{r}_p\}). \tag{32}$$

Following this second approach, the evolution of the contours is governed by a set of differential equations for the coefficients $\{C_\alpha\}$:

$$\frac{dC_\alpha}{dt} = \sum_{p=1}^{N} \frac{\partial h_\alpha}{\partial \mathbf{r}_p} \cdot \mathbf{v}_p = \sum_{p=1}^{N} \frac{\partial h_\alpha}{\partial \mathbf{r}_p} \cdot \mathbf{g}(\mathbf{r}_p, \{C_\beta\}), \quad \alpha = 1, \ldots N_c. \tag{33}$$

In the present paper the first approach has been followed (essentially for its simplicity). However, the second technique, which could also allow help develop semianalytic studies (e.g., by generalizing the method proposed by Fine [9]), is in principle more general and further investigations should focus on it.

3. CONTOUR DESCRIPTION AND NUMERICAL EVALUATION OF CONTOUR INTEGRALS

By using formulas (8), one can verify that the image of a line segment AB within the trap is the arc $A'B'$, shown in Fig. 1, of a circle passing through the center of the trap with radius $R_c = R^2/2d$, where d is the distance of the segment from the center of the trap. The length of the arc is

$$\Delta l_a = 2R_c|\theta_1 - \theta_2|, \tag{34}$$

where θ_1, θ_2 are the azimuthal coordinates of the end points of the segment. Thus, by adopting a polygonal description of the contours of the real vortices, the image contours are determined exactly.

To evaluate the contour integrals (14), (21a), and (21b), a numerical approach is required. In the present work, the following discretization scheme, for a generic function $Z(\mathbf{r}, \mathbf{r}')$, has been adopted:

$$\oint_{\partial D} Z(\mathbf{r}, \mathbf{r}')\, dl' \simeq \sum_{j=1}^{N_l} Z(\mathbf{r}, \bar{\mathbf{r}}'_j)\Delta l_j \tag{35a}$$

$$\oint_{\partial \hat{D}} Z(\mathbf{r}, \mathbf{r}')\, dl' \simeq \sum_{j=1}^{N_l} Z(\mathbf{r}, \bar{\mathbf{r}}'_{aj})\Delta l_{aj}. \tag{35b}$$

Here $\bar{\mathbf{r}}'_j$, Δl_j, $\bar{\mathbf{r}}'_{aj}$, and Δl_{aj} are the medium points and the lengths of the segments of the real contour and of the arcs of the image contour, respectively.

When a segment approaches the center of the trap, the length of its corresponding image arc increases and this numerical scheme may appear to be inconvenient. Actually, recalling formulas (8) and (10), one can show that, for the contour integrals (14), (21a), and (21b), $Z(\mathbf{r}, \bar{\mathbf{r}}'_{aj})\Delta l_{aj}$ behaves asymptotically as $1/\bar{r}'^3_{aj}$ when $\bar{r}'_{aj} \to \infty$, providing a negligible contribution to the integral: Thus, a bad estimation does not lead to a significant error.

By using formulas (35a) and (35b), the velocity of each node on the contours is readily calculated and the position of the nodes is updated using a second-order Runge–Kutta

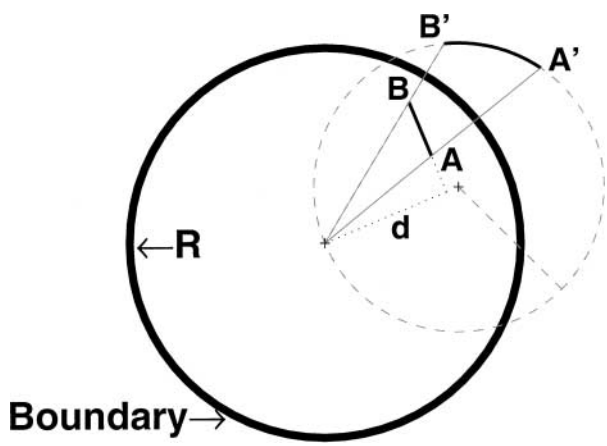

FIG. 1. Segment of the real contour and corresponding image arc.

method, in which the value of each time step, Δt, is determined consistently with the contour discretization, by imposing that the maximum displacement $|\mathbf{v}_{\max}|\Delta t$ be smaller than the minimum length of the segments.

To maintain good precision in the polygonal description of the contour, a redistribution routine is required. In fact, if the shape of a vortex grows in complexity during a simulation, a good description of its contour can be achieved only by increasing the number of nodes N. On the other hand, N should be maintained as low as possible to obtain good efficiency of the algorithm, as the computational time is proportional to N^2. Therefore, some nodes must be eliminated when they are so close to one another that the error introduced by their elimination is negligible.

The redistribution routine operates at each time step: It controls both the length of each side of every polygon and the curvature in each node, in order to identify where the contours have to be refined. By doing so, the contour is modified only where necessary and hence nonphysical contour perturbations, generally caused by the redistribution, are drastically reduced.

The length ΔL of each side of the polygon is compared with a predefined minimum length $\Delta L_{\min}$: If $\Delta L < \Delta L_{\min}$, the end points are eliminated and a new point is inserted in the middle of the old segment. A second control is carried out by comparing the length ΔL of each side with a maximum length $\Delta L_{\max}(k)$, defined as a function of the local curvature k: If $\Delta L > \Delta L_{\max}(k)$, a new node is inserted in the middle of the segment. Thus, to increase the local linear density of nodes in high curvature regions, $\Delta L_{\max}(k)$ must be a decreasing function of the curvature k. With reference to Dritschel's work [3], the expression

$$\Delta L_{\max}(k) = b + \frac{c}{k^p} \tag{36}$$

has been used, with a suitable choice of coefficients b, c, and p. The spatial resolution of the CD code and, consequently, the precision reached in the contour description depend only on the choice of $\Delta L_{\min}$ and $\Delta L_{\max}(k)$, whose optimal values are in general different when referred to distinct vortices: For this reason, the routine is self-adaptive with respect to the characteristic dimension of each vortex. More details on this issue are presented in the Appendix.

4. RESULTS AND CONCLUSIONS

To prove the effectiveness of the proposed method, numerous simulations have been carried out. In the following, results are presented for two different "classic" phenomena: (a) the instability for hollow density profiles and (b) the interaction between vortices. The results show the very precise contour description provided by the CD algorithm even when the shape of the vortices reaches a high level of complexity. The precision of the results has been checked by changing the number of nodes and/or decreasing the time step; in some cases, they have been compared with PIC simulations. For this reason, they can be regarded as reference results for the physical problem considered.

In the following, dimensionless units are used, in which $R = 1$, $B_0 = 1$, and $\varepsilon_0 = 1$. Figures 2 and 3 report some frames of the evolution of a perturbed plasma ring,

$$\rho(r, \theta) = \begin{cases} 1000, & r_1(\theta) < r < r_2(\theta) \\ 0, & \text{otherwise,} \end{cases} \tag{37}$$

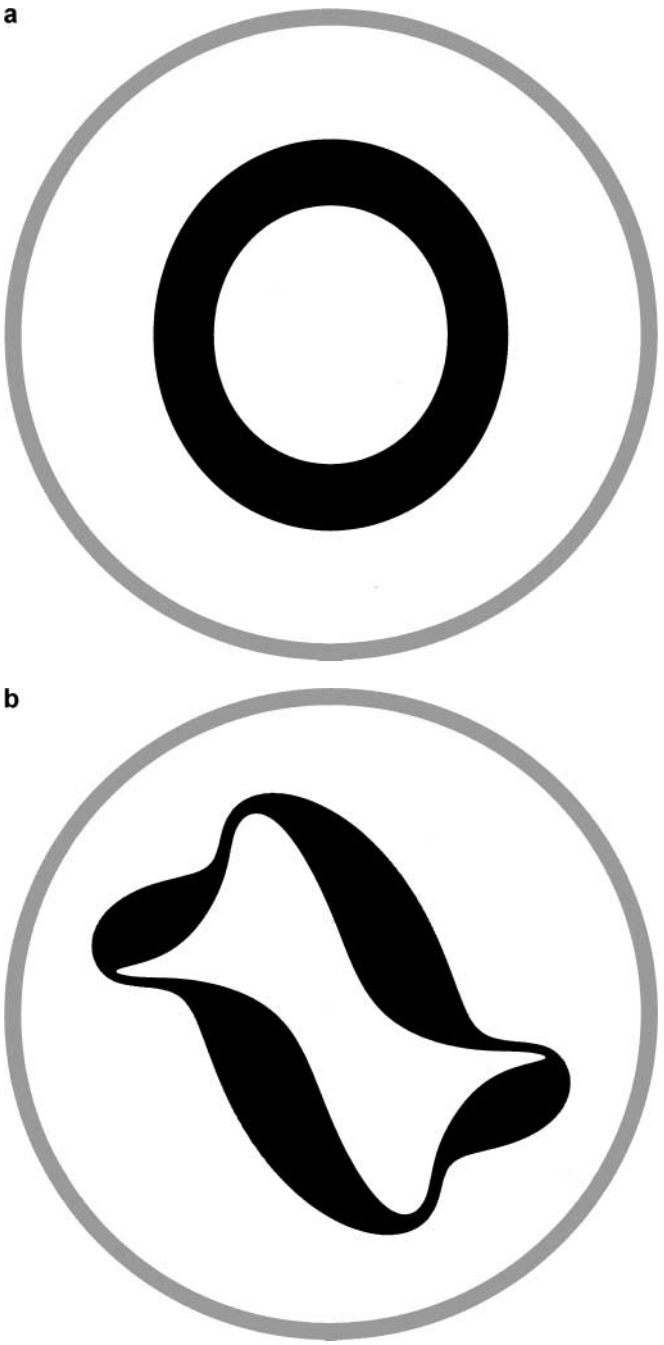

FIG. 2. Evolution of a plasma ring perturbed according to Eqs. (37) and (38) with $m = 2$: (a) initial distribution, (b) distribution at $t = 3.893 \times 10^{-2}$, (c) distribution at $t = 5.188 \times 10^{-2}$, and (d) distribution at $t = 6.010 \times 10^{-2}$. The level of accuracy is obtained by setting $N_{\text{ref}} = 128$.

FIG. 2—*Continued*

where

$$r_1(\theta) = 0.4[1 + 0.05\cos(m\theta)], \quad r_2(\theta) = 0.6[1 + 0.05\cos(m\theta)] \tag{38}$$

for $m = 2$ (Fig. 2) and $m = 3$ (Fig. 3). The results presented are in excellent agreement with the analytic results obtained from a linear analysis of stability [5].

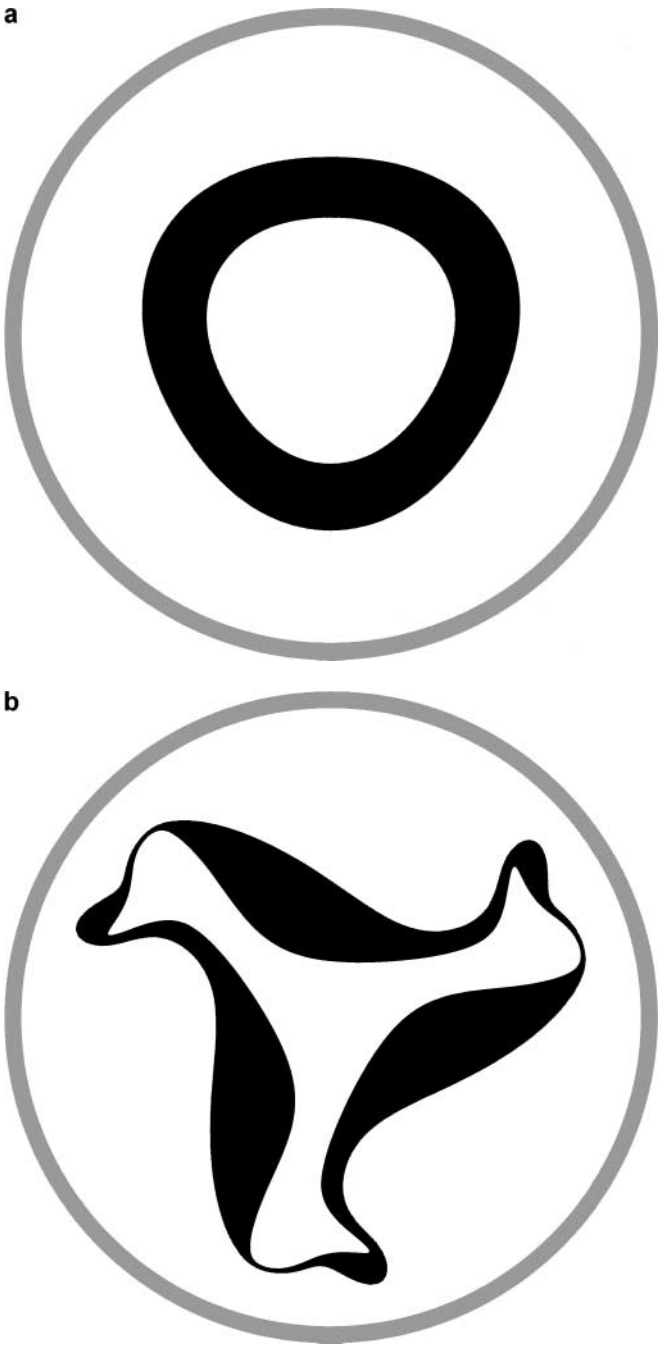

FIG. 3. Evolution of a plasma ring perturbed according to Eqs. (37) and (38) with $m = 3$ ($N_{\text{ref}} = 128$): (a) initial distribution, (b) distribution at $t = 2.913 \times 10^{-2}$, (c) distribution at $t = 3.832 \times 10^{-2}$, and (d) distribution at $t = 5.114 \times 10^{-2}$.

Figures 4–8 show the evolution of two-ring patterns of vortices of finite size, which extend the point-vortex studies published in Refs. [10, 11]. A six-vortex configuration has been considered: The inner and the outer rings have radii $R_1 = 0.35$ and $R_2 = 0.5$, respectively, with $\rho_1 = 2917$ and $\rho_2 = 1000$ (the radius of each vortex is $r = 0.1$). This pattern would be

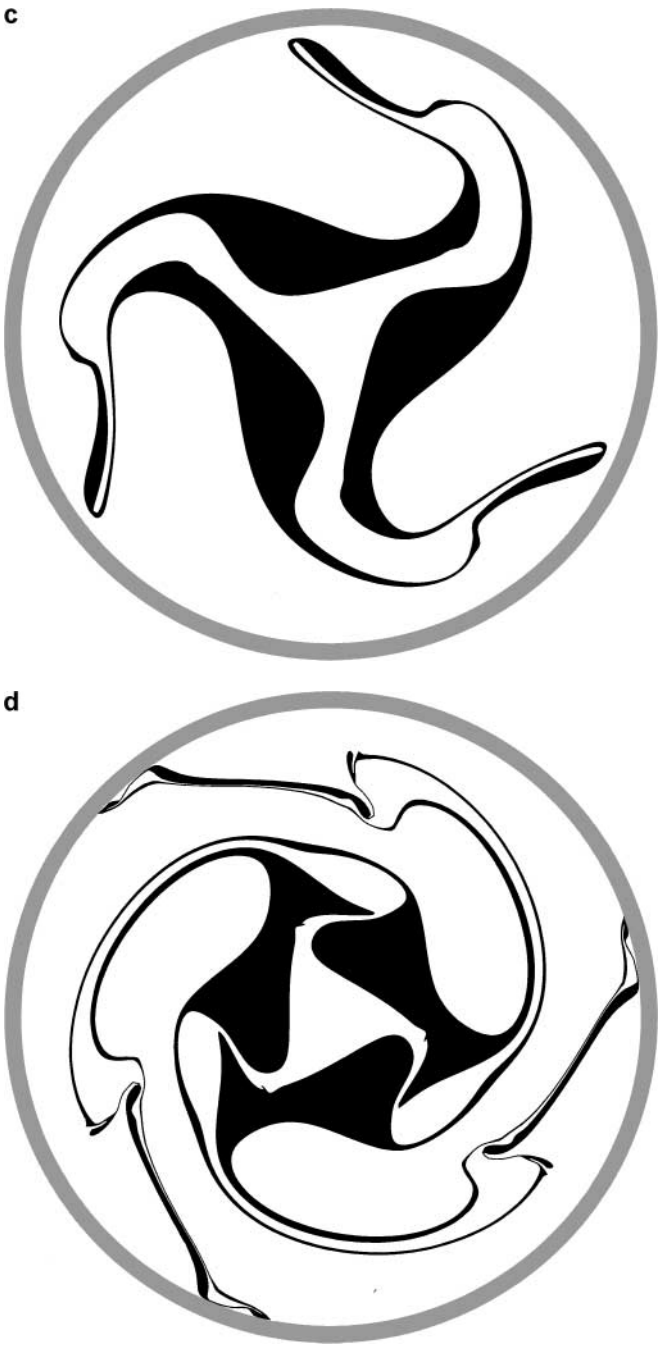

FIG. 3—*Continued*

an equilibrium configuration in the framework of the point-vortex theory [10]. In contrast, when circular vortices of relevant dimensions are taken into account, the shape of the outer vortices keeps changing in time and very long, thin filaments are generated (Fig. (4)).

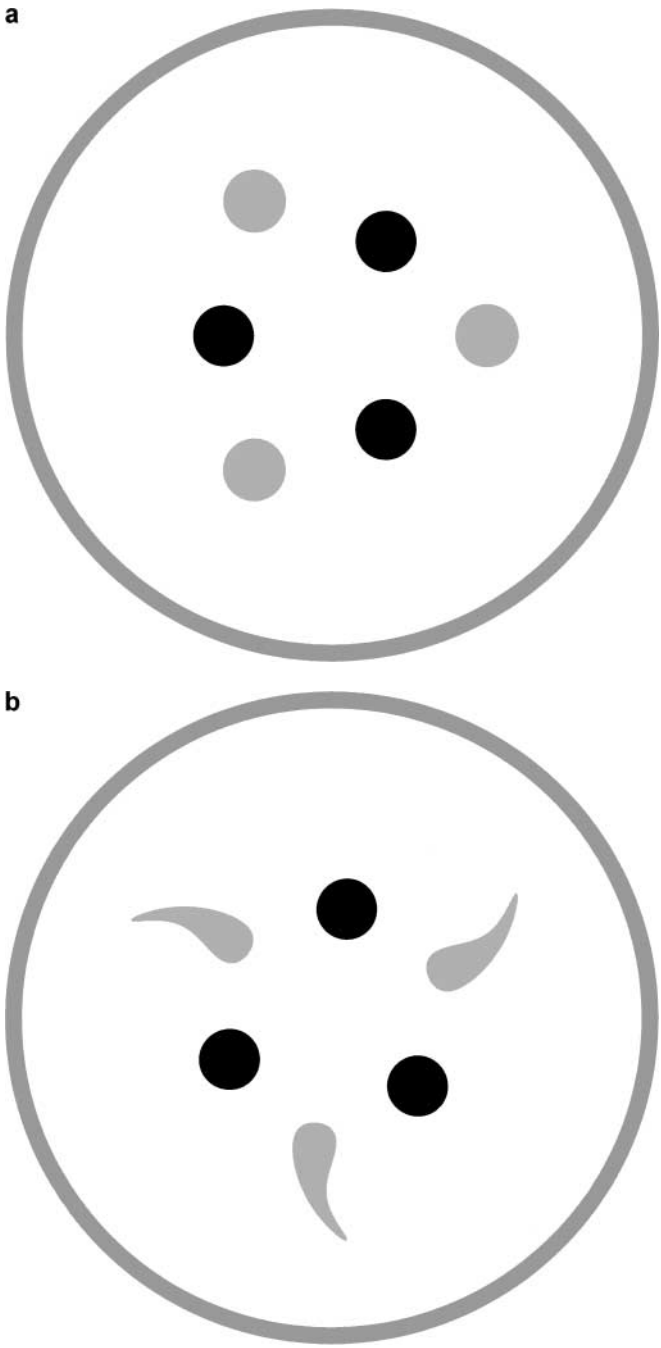

FIG. 4. Evolution of a two-ring pattern of vortices with radius $r = 0.1$ ($N_{\text{ref}} = 128$): (a) initial configuration, (b) distribution at $t = 2.512 \times 10^{-2}$, (c) distribution at $t = 4.522 \times 10^{-2}$, and (d) distribution at $t = 5.667 \times 10^{-2}$.

A different case has been studied in the second simulation by setting $R_1 = 0.32$, $R_2 = 0.55$ and taking into account circular vortices of radius 0.2 and the same densities. In addition to the CD technique, the simulation has been carried out also using a PIC code [6] with a very fine mesh for the polar grid ($\Delta r = R/450$, $\Delta\theta = 2\pi/512$) and 6×10^5 particles.

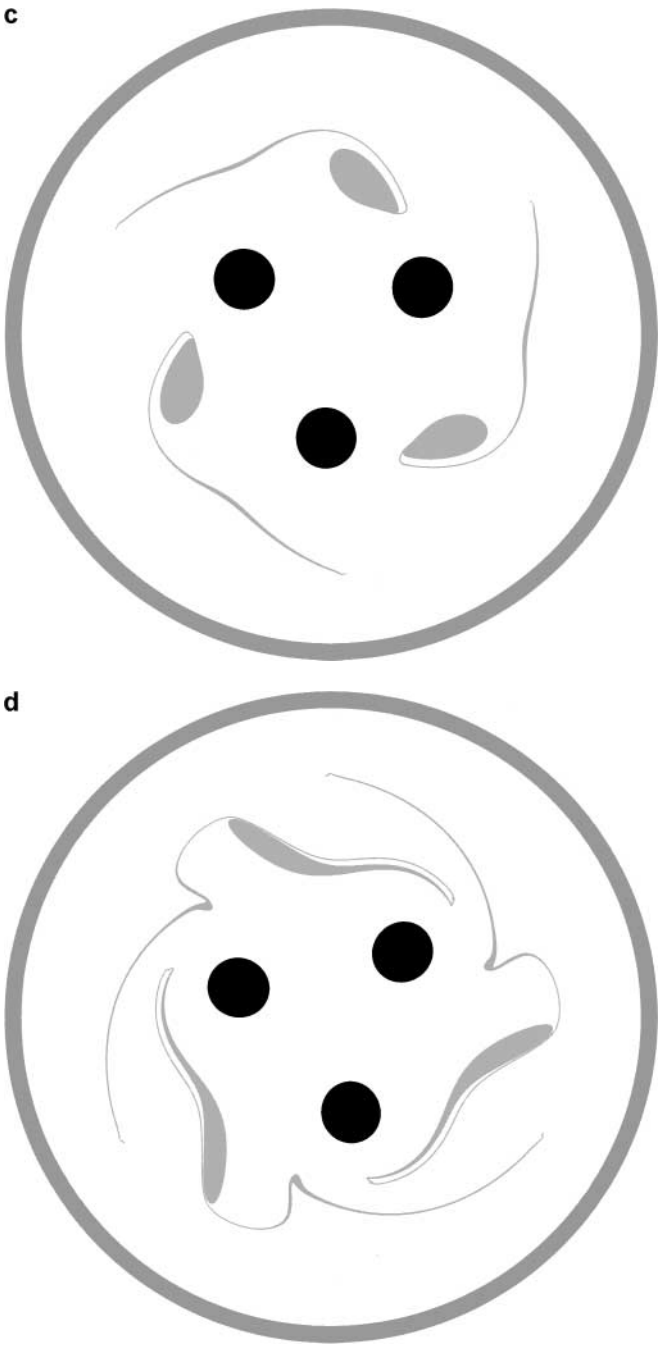

FIG. 4—*Continued*

Four frames of the evolution obtained with the CD technique are reported in Fig. 5. In Figs. 6–8 the CD results are compared both with the ones provided by the PIC code and with the results of the CD code set for lower precision (see the Appendix). Figure 9 shows the growth of the total number of nodes, N, for the two CD simulations. All the results

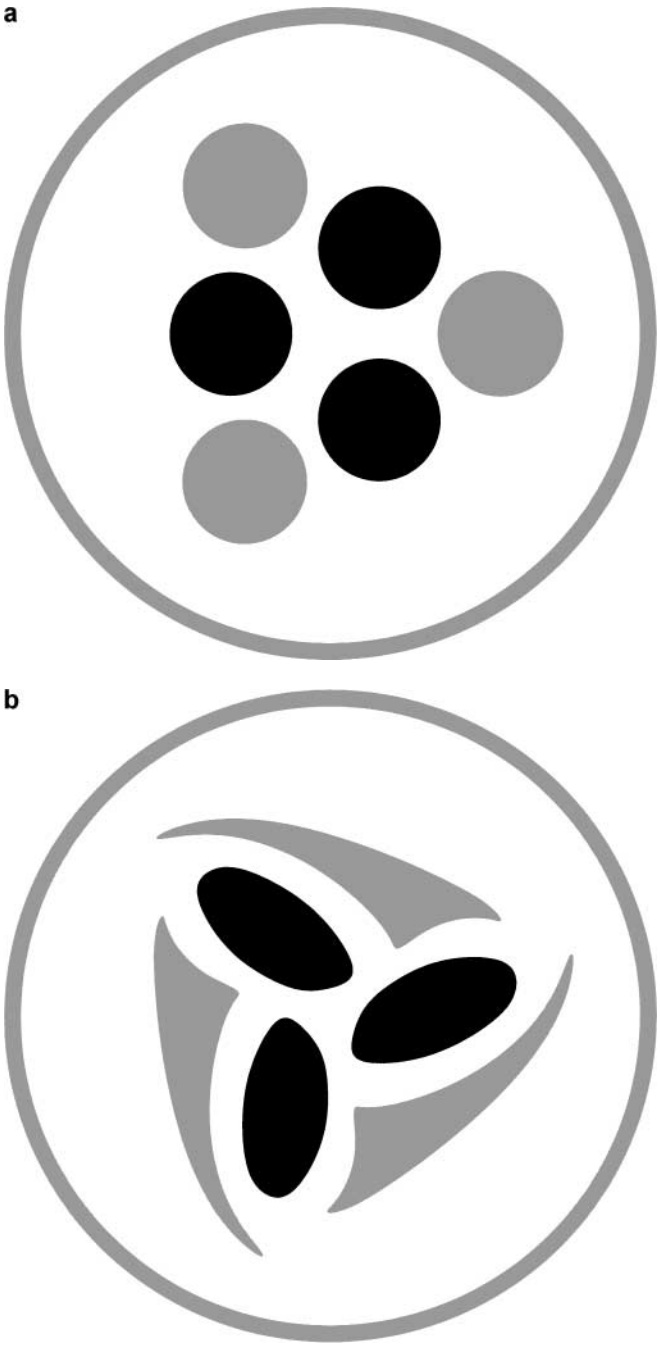

FIG. 5. Evolution of a two-ring pattern of vortices with radius $r = 0.2$ ($N_{\text{ref}} = 128$): (a) initial configuration, (b) distribution at $t_b = 0.479 \times 10^{-2}$, (c) distribution at $t_c = 1.004 \times 10^{-2}$, and (d) distribution at $t_d = 1.462 \times 10^{-2}$.

clearly show the excellent agreement between the two different techniques and the high level of precision of the CD method.

The CD code set for lower resolution required nearly one-half the time T_{PIC} taken by the PIC code, while the more accurate CD technique required a total computational time

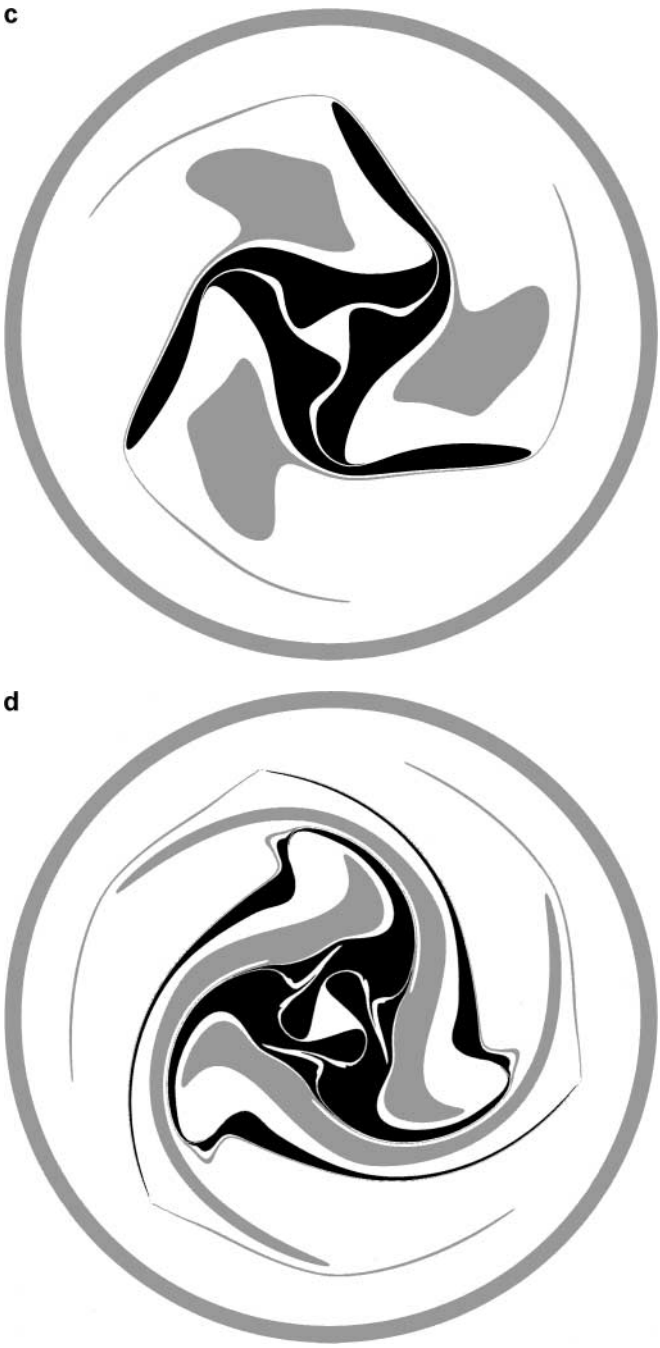

FIG. 5—*Continued*

of nearly $4T_{\mathrm{PIC}}$. A rigorous comparison between the computational cost of the PIC method and that of the CD method is difficult to make, as one should define a common criterion of accuracy for completely different techniques, and this goes beyond the purposes of the present work.

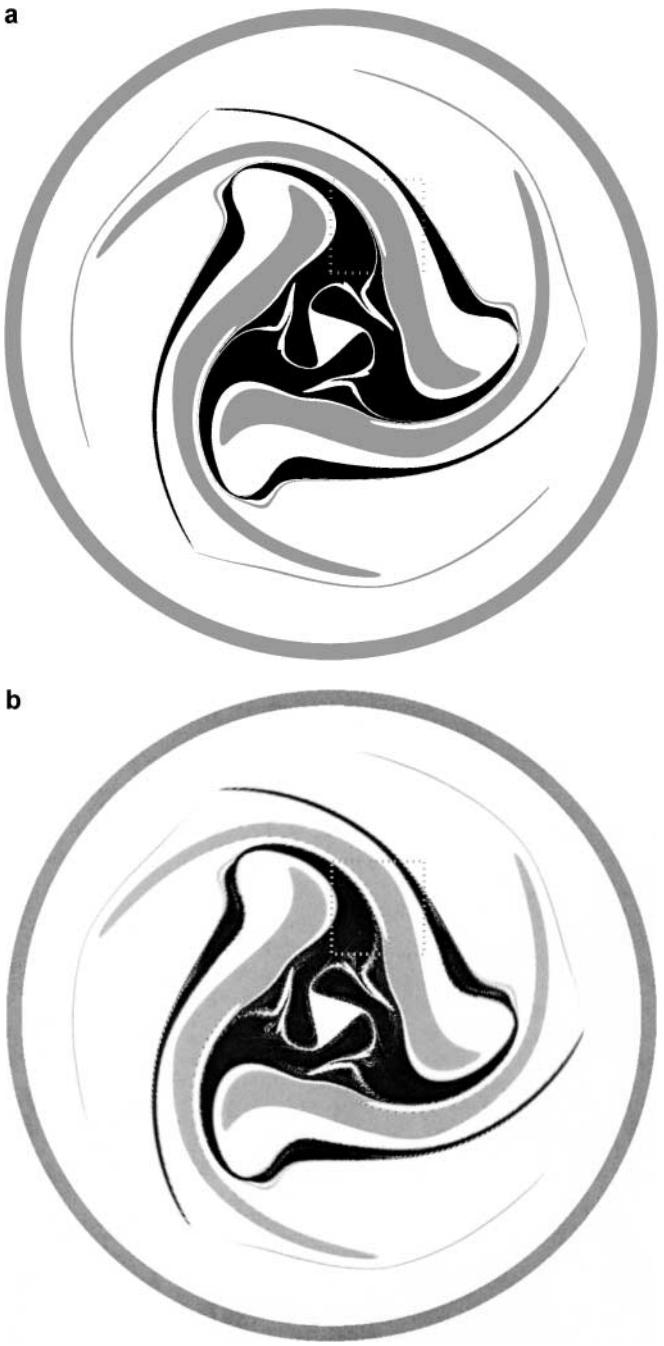

FIG. 6. Comparison between the two distributions obtained with (a) CD ($N_{\text{ref}} = 128$) and (b) PIC at time $t = 1.402 \times 10^{-2}$.

As far as the CD method developed by Backhaus *et al.* [7, 8] is concerned, one can observe that its precision depends both on the number N of points of the contour and on the number L of boundary points in which the field ϕ_p is evaluated. At each time step, the computational costs to evaluate ϕ_p, the coefficients $\{D_l\}$, and ϕ_0 are proportional to

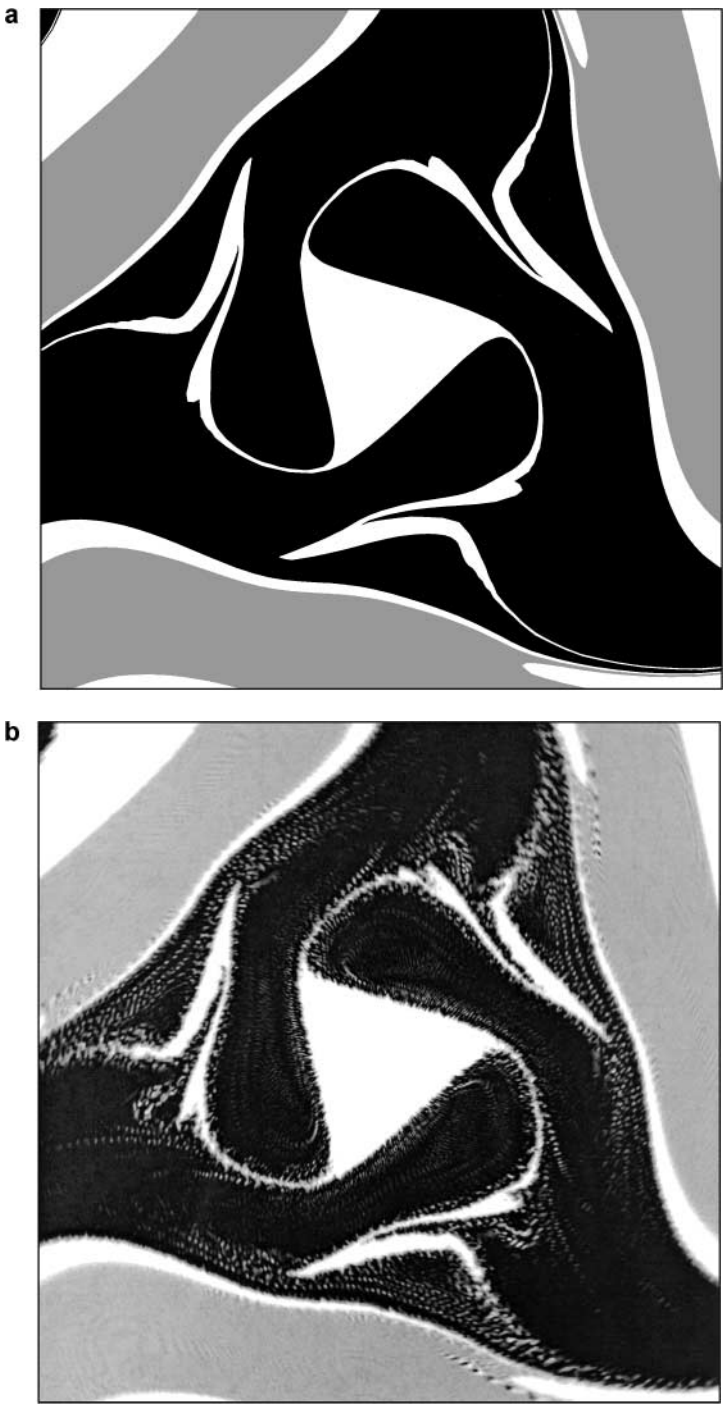

FIG. 7. A detail of the central part of the charge density distribution at time $t = 1.402 \times 10^{-2}$, obtained with (a) the CD code ($N_{\text{ref}} = 128$), (b) the PIC code, and (c) the CD code set for lower resolution ($N_{\text{ref}} = 64$).

FIG. 7—*Continued*

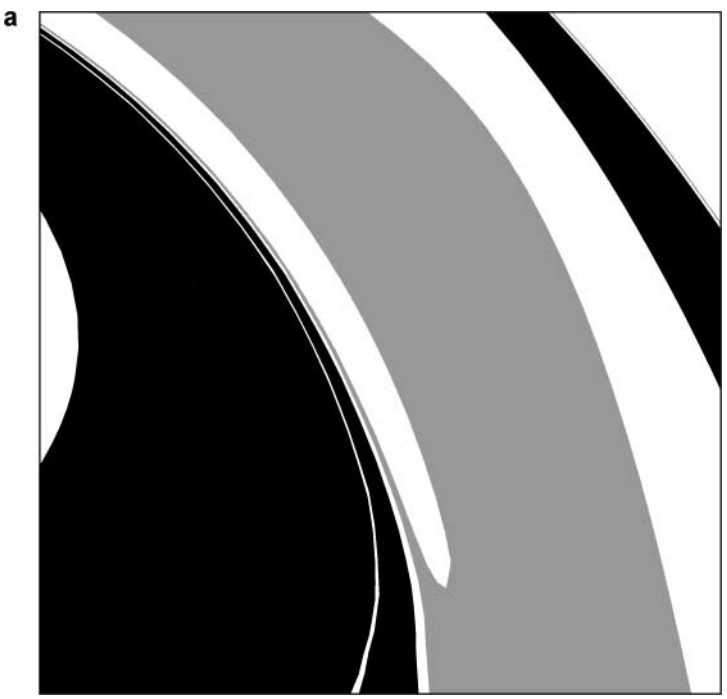

FIG. 8. A detail of the region marked by a dotted line in Fig. 6, obtained with (a) the CD code ($N_{\text{ref}} = 128$), (b) the PIC code, and (c) the CD code set for lower resolution ($N_{\text{ref}} = 64$).

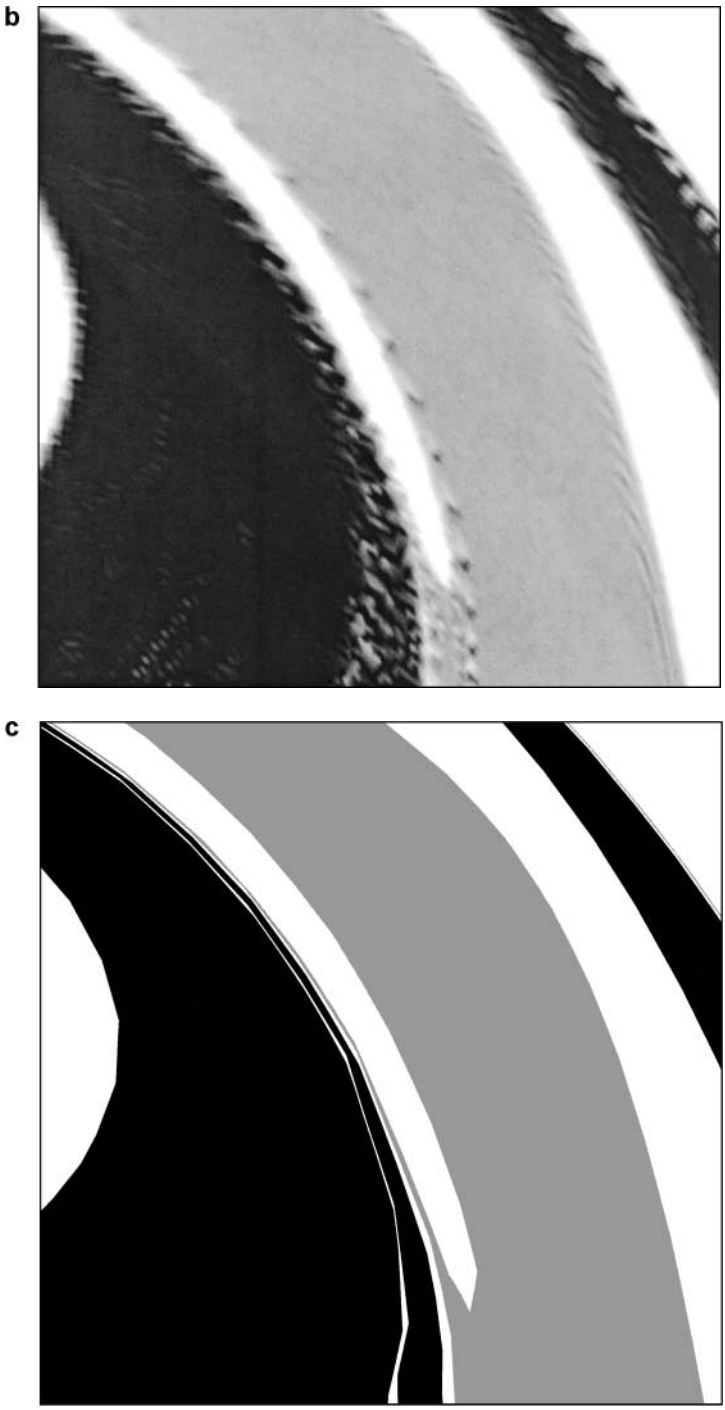

FIG. 8—*Continued*

$N(N+L)$, $L\log_2 L$, and NL, respectively. From these considerations, one can guess that, for standard precision, the two CD methods are nearly equally time consuming. In contrast, when high precision is required, L must be increased much more with respect to N (in fact, $\Delta\theta = 2\pi/L$ is constant, while the contour must be refined only in some regions of the

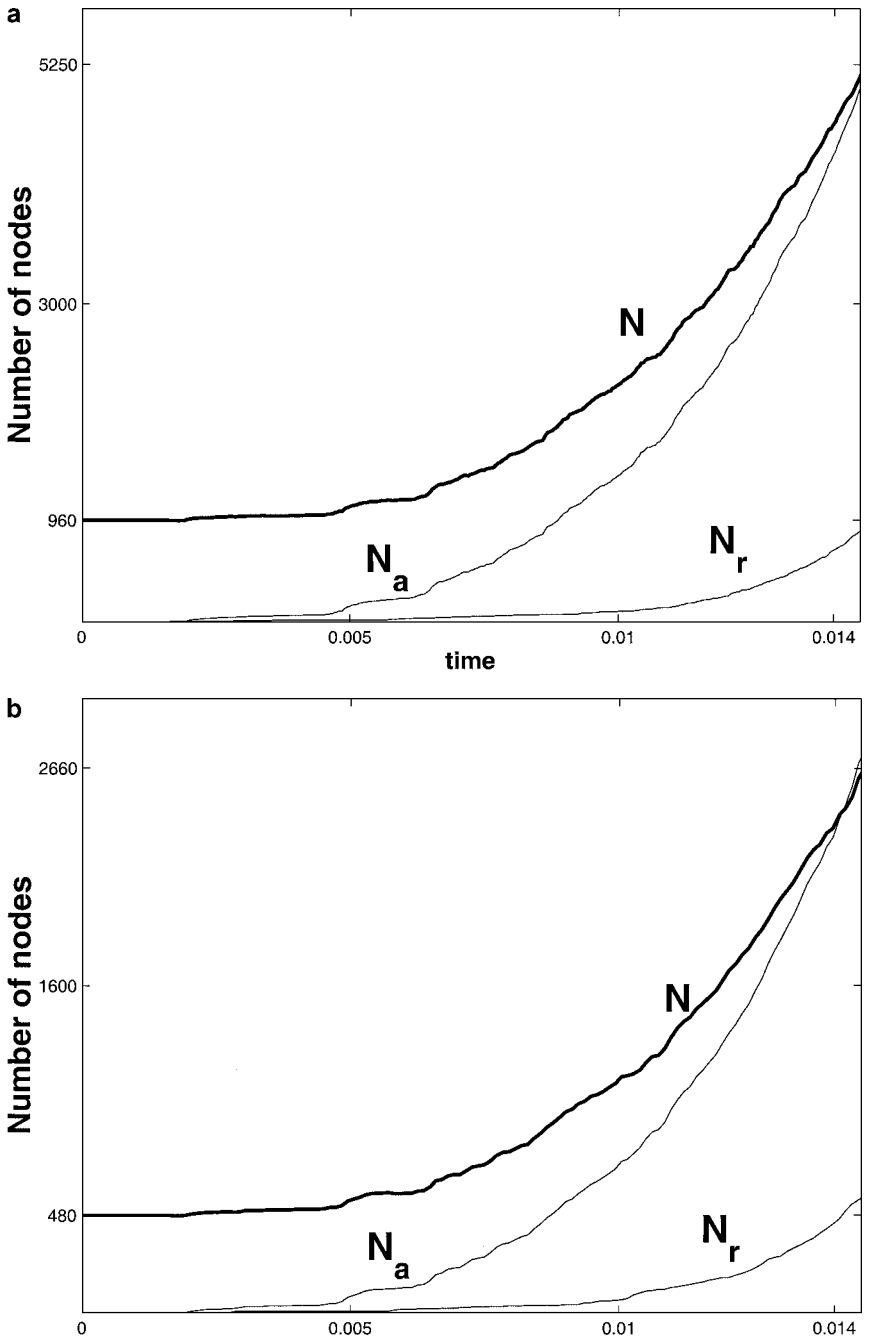

FIG. 9. Evolution of the total number of nodes (N), of the number of added nodes (N_a), and of the number of removed nodes (N_r), setting (a) $N_{ref} = 128$ and (b) $N_{ref} = 64$.

vortices; thus, a contour described by a relatively small number of nodes could require a large number of boundary nodes): In this case, the effectiveness of Backaus's method is reduced.

The extremely high precision obtained with the CD method presented here depends mainly on the analytic expression for the velocity field. Moreover, a proper treatment of

the contours by means of an optimized redistribution routine is required. Future work will focus on the study of more efficient methods for evaluating the contour integrals to reduce the number of nodes and, consequently, the computational effort.

The code based on the CD algorithm has also been used for other studies on nonneutral plasmas; Although results are not reported here, they are worth mentioning. For instance, the code has been adapted to study the interaction between vortices of finite size and point vortices, as it is very effective in describing the merging processes which are typical of such configurations [12]. In particular, results of the CD code have been compared with those obtained with a generalization of the analytic analysis proposed by Coppa *et al.* [13].

A more ambitious application of the code is the simulation of a non-neutral plasma in the framework of recently developed kinetic models [14, 15]. According to these models, electrons of different energy $\mathcal{E}$ "feel" a different z-averaged electric field (depending on the different penetration depth of the particles in the end-electrode regions) and, consequently, the $\mathbf{E} \times \mathbf{B}$ drift law must be modified as

$$\mathbf{v}(r, \theta, \mathcal{E}) = \frac{\alpha(\mathcal{E})}{B_0} \hat{\mathbf{e}}_z \times \frac{\partial \phi(r, \theta)}{\partial \mathbf{r}}, \tag{39}$$

where $\alpha(\mathcal{E})$ is a suitable function of the energy, to be determined self-consistently [16]. Therefore, a plasma distribution which is represented as a single vortex within the standard model must be considered as a superposition of vortices of different energy, each evolving according to Eq. (39). Work is in progress on this issue.

APPENDIX: CONTROL OF THE ACCURACY

As shown in Section 3, good accuracy in the contour description, for the whole simulation, requires a proper choice of the bounds on line segment lengths. This means that, for each vortex, the function $\Delta L_{\max}(k)$ and the value of $\Delta L_{\min}$ have to be chosen, depending on the initial shape of the vortex. The algorithm presented here provides an automatic setting of all the redistribution parameters.

First, for each vortex, a characteristic length, R_{eq}, is evaluated as

$$R_{\text{eq}} = \left(\frac{A}{\pi} \right)^{\frac{1}{2}}, \tag{40}$$

where A is the area of the vortex Then, one can define a reference curvature value, $k_{\text{ref}} = 1/R_{\text{eq}}$ and a reference segment length,

$$\Delta L_{\text{ref}} = \frac{2\pi R_{\text{eq}}}{N_{\text{ref}}}, \tag{41}$$

where N_{ref} is the number of nodes one should use to describe a circle with the required spatial resolution. In dimensionless units, formula (36) for $\Delta L_{\max}(\hat{k})$ can now be rewritten as

$$\Delta \hat{L}_{\max}(\hat{k}) = \hat{b} + \frac{\hat{c}}{\hat{k}^p}, \tag{42}$$

where

$$\Delta\hat{L}_{\max}(\hat{k}) = \frac{\Delta L_{\max}(\hat{k})}{\Delta L_{\text{ref}}}, \quad \hat{k} = \frac{k}{k_{\text{ref}}}. \tag{43}$$

Once N_{ref} is fixed, contours of vortices having the same area are described with the same spatial resolution, as ΔL_{ref} and $\Delta L_{\max}(k)$ depend only on R_{eq}. The initial number of nodes N on each contour is determined by setting the mean segment length, $\overline{\Delta L}$, equal to ΔL_{ref}; this leads to

$$N \cong \frac{P}{2\pi R_{\text{eq}}} N_{\text{ref}}, \tag{44}$$

where P is the perimeter of the vortex. In this way, the accuracy of the method depends only on N_{ref}.

After several tests on the redistribution routine, the following values for the parameters in formula (42) have been chosen:

$$\hat{b} = 0.15, \quad p = 0.7, \quad \hat{c} = 1.6. \tag{45}$$

Furthermore, to prevent the linear density of nodes from increasing without control in regions of high curvature, a lower bound for $\Delta\hat{L}_{\max}(\hat{k})$ has been introduced; on the other hand, to mantain good accuracy where the curvature is low, an upper bound is also necessary. Eventually, the expression

$$\Delta\hat{L}_{\max}(\hat{k}) = \begin{cases} 2, & \hat{k} < \hat{k}_1 \\ \hat{b} + \dfrac{\hat{c}}{\hat{k}^p}, & \hat{k}_1 \le \hat{k} < 3 \\ \hat{b} + \dfrac{\hat{c}}{3^p}, & \hat{k} \ge 3 \end{cases} \tag{46}$$

is adopted, with

$$\hat{k}_1 = \left[\frac{\hat{c}}{(2-\hat{b})}\right]^{\frac{1}{p}}. \tag{47}$$

The minimum acceptable segment length $\Delta\hat{L}_{\min}$ is set as a fraction of the lower bound of $\Delta\hat{L}_{\max}(\hat{k})$, with the constraint

$$\Delta\hat{L}_{\min} < \frac{1}{2}\left(\hat{b} + \frac{\hat{c}}{3^p}\right); \tag{48}$$

in this way, the insertion of a node does not generate segments that are too short.

In the present implementation of the method, $\Delta L_{\min}$ and all the parameters appearing in $\Delta L_{\max}(k)$ are defined for each vortex once at the beginning of the simulation and remain constant in time. As a future development, one may try to improve the accuracy of the contour description during the simulation when necessary, by changing dynamically N_{ref}. In this case a more efficient contour description (for instance using cubic interpolation between nodes, as in Ref. [3]) would be recommended to reduce the computational effort.

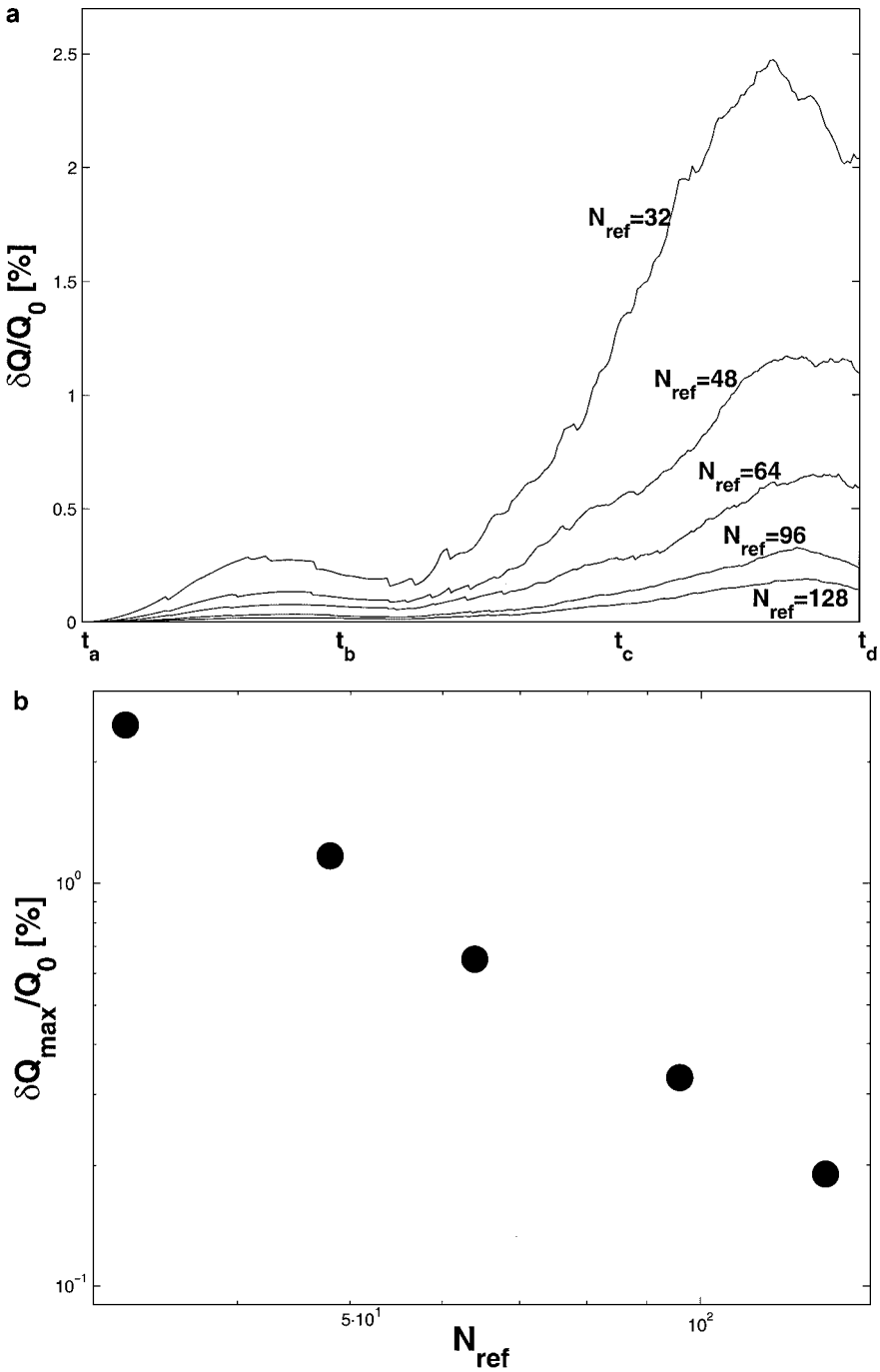

FIG. 10. (a) Evolution of the total charge for the case of Fig. 5, with different values of N_{ref}. (b) Maximum percentage deviation of the total charge from its initial value, with the considered set of N_{ref}.

To show the importance of the parameter N_{ref} on the precision achieved with this CD technique, the evolution of the same pattern of vortices (Figs. 4–8) has been calculated for five different values of N_{ref} (Fig. 10). For each case, the total charge of the distribution (which according to the theory should be constant) has been calculated, at different times

during the simulation, as

$$Q = \sum_{i=1}^{N_v} \rho_i \int\int_{D_i} dx\, dy = \sum_{i=1}^{N_v} \rho_i \oint_{\partial D_i} x n_x\, dl \simeq \sum_{i=1}^{N_v} \rho_i \left(\sum_{j=1}^{(N_l)_i} \bar{x}_j n_{xj} \Delta l_j \right), \qquad (49)$$

where N_v is the number of vortices, ρ_i is the charge density of the ith vortex, $\bar{x}_j$ is the x coordinate of the medium point of the jth segment, and n_{xj} is the x-component of the normal unit vector.

The deviation of Q from its initial value can be regarded as a relative measure of the accuracy attained in the simulation. Figures 10a and 10b report the evolution in time of the relative deviation of the total charge δQ and the maximum relative deviation, $\delta Q_{\max}/Q_0$, for each value of N_{ref}, respectively.

Clearly, the parameter N_{ref} affects the computational cost required by this CD algorithm: In fact, it can be shown that the mean computational cost per time step is proportional to N_{ref}^2, while the number of time steps is proportional to N_{ref}: This makes the total simulation time proportional to N_{ref}^3.

ACKNOWLEDGMENTS

The authors thank Antonio D'Angola and Gian Luca Delzanno for many useful discussions and for help with the PIC simulations.

REFERENCES

1. G. S. Deem and N. J. Zabusky, Vortex waves: Stationary "V states," interactions, recurrence and breaking, *Phys. Rev. Lett.* **40**, 859 (1978).
2. N. J. Zabusky, M. H. Hughes, and K. V. Roberts, Contour dynamics for the Euler equations in two dimensions, *J. Comput. Phys.* **30**, 96 (1979).
3. D. G. Dritschel, Contour dynamics and contour surgery: Numerical algorithms for extended, high-resolution modelling of vortex dynamics in two-dimensional, inviscid, incompressible flows, *Comput. J. Phys. Rep.* **10**, 77 (1989).
4. R. D. Van Buskirk and P. S. Marcus, Spectrally accurate contour dynamics, *J. Comput. Phys.* **115**, 302 (1994).
5. R. Davidson, *An Introduction to the Physics of Nonneutral Plasmas* (Addison-Wesley, Redwood City, CA, 1990).
6. G. G. M. Coppa, A. D' Angola, and G. Lapenta, Simulation of the evolution of the diocotron instability, in *Workshop on Non-Neutral Plasmas, Princeton, New Jersey USA, August 1999, Non-Neutral Plasma Physics III*, edited by J. J. Bollinger, R. L. Spencer, and R. C. Davidson (American Institute of Physics, Conference Proceedings 498, Melville, NY, 1999), pp. 129–134.
7. E. Yu. Backhaus, J. Fajans, and J. S. Wurtele, Application of contour dynamics to systems with cylindrical boundaries, *J. Comput. Phys.* **145**, 462 (1998).
8. E. Yu. Backhaus, J. Fajans, and J. S. Wurtele, Stability of highly asymmetric non-neutral plasmas, *Phys. Plasmas* **6**, 19 (1999).
9. K. S. Fine, Simple theory of a nonlinear diocotron mode, *Phys. Fluids B* **4**, 3981 (1992).
10. G. G. M. Coppa, Analytic studies of two-ring patterns of vortices in a Penning trap, in *Workshop on Non-Neutral Plasmas, Princeton, New Jersey USA, August 1999, Non-Neutral Plasma Physics III*, edited by J. J. Bollinger, R. L. Spencer, and R. C. Davidson (American Institute of Physics, Conference Proceedings 498, Melville, NY, 1999), pp. 123–128.

11. D. Durkin, L. Zimmerman, and J. Fajans, A selection of experiments performed with the photocathode trap, in *Workshop on Non-Neutral Plasmas, Princeton, New Jersey USA, August 1999, Non-Neutral Plasma Physics III*, edited by J. J. Bollinger, R. L. Spencer, and R. C. Davidson (American Insitute of Physics, Conference Proceedings 498, Melville, NY, 1999), pp. 93–98.
12. I. M. Lansky, T. M. O'Neil, and D. A. Schecter, A theory of vortex merger, *Phys. Rev. Lett.* **79**, 1479 (1997).
13. G. G. M. Coppa, A. D' Angola, F. Peano, and F. Peinetti, Analysis of vortex merger in systems with cylindrical boundaries, to be published.
14. G. G. M. Coppa and P. Ricci, Non-collisional kinetic model for non-neutral plasmas in a Penning trap: General properties and stationary solutions, *Phys. Rev. E*, to appear.
15. T. J. Hilsabeck and T. M. O'Neil, Finite length diocotron modes, *Phys. Plasmas* **8**, 407 (2001).
16. A. J. Peurrung and J. Fajans, A limitation to the analogy between pure electron plasmas and two-dimensional inviscid fluids, *Phys. Fluids B* **5**, 4295 (1993).